



HAL
open science

Degradable Hollow Organosilica Nanoparticles for Antibacterial Activity

Saher Rahmani, Karim Bouchmella, Jelena Budimir, Laurence Raehm, Mateus Borba Cardoso, Philippe Trens, Jean-Olivier Durand, Clarence Charnay

► **To cite this version:**

Saher Rahmani, Karim Bouchmella, Jelena Budimir, Laurence Raehm, Mateus Borba Cardoso, et al.. Degradable Hollow Organosilica Nanoparticles for Antibacterial Activity. ACS Omega, 2019, 4 (1), pp.1479-1486. 10.1021/acsomega.8b02779 . hal-02047845

HAL Id: hal-02047845

<https://hal.science/hal-02047845>

Submitted on 25 May 2021

HAL is a multi-disciplinary open access archive for the deposit and dissemination of scientific research documents, whether they are published or not. The documents may come from teaching and research institutions in France or abroad, or from public or private research centers.

L'archive ouverte pluridisciplinaire **HAL**, est destinée au dépôt et à la diffusion de documents scientifiques de niveau recherche, publiés ou non, émanant des établissements d'enseignement et de recherche français ou étrangers, des laboratoires publics ou privés.

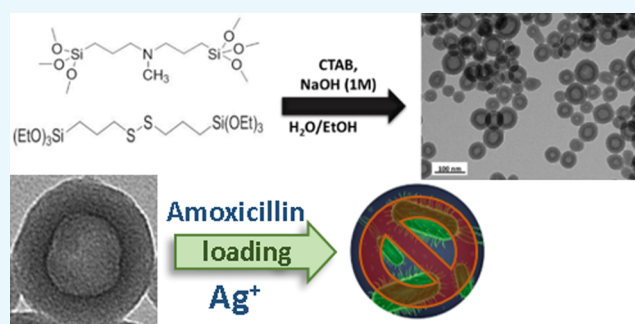
Degradable Hollow Organosilica Nanoparticles for Antibacterial Activity

Saher Rahmani,[†] Karim Bouchmella,[‡] Jelena Budimir,[†] Laurence Raehm,[†] Mateus Borba Cardoso,[‡] Philippe Trens,[†] Jean-Olivier Durand,[†] and Clarence Charnay^{*,†}

[†]Institut Charles Gerhardt Montpellier, UMR-5253 Univ Montpellier, CNRS, ENSCM, cc 1701, Place Eugène Bataillon, 34095 Montpellier Cedex 05, France

[‡]Laboratório Nacional de Nanotecnologia (LNNano) e Laboratório Nacional de Luz Síncrotron, Centro Nacional de Pesquisa em Energia e Materiais (CNPEM), CEP 13083-970, Campinas, São Paulo, Brazil

ABSTRACT: The synthesis of hollow organosilica nanoparticles is described from bis triethoxysilylpropyl disulfide and bis(trimethoxysilylpropyl)methylamine. The nanoparticles were monodisperse with a mean diameter of 90 nm, and the adsorption–desorption properties of these nanoparticles were investigated with nitrogen at 77 K, *n*-hexane, and water. The nanoparticles were nonporous at 77 K as shown by N₂ sorption analyses. *n*-Hexane interacted reversibly through physisorption with the nanoparticles, whereas water showed a strong nonreversible interaction, probably because of chemisorption with nitrogen atom sites. Amoxicillin antibiotic was loaded with these nanoparticles and the loading capacity was 30%. Ag⁺ ions were also adsorbed with amoxicillin, and the multifunctional nanoparticles were efficient in inhibiting bacterial growth with a synergy between the antibiotic delivery and Ag⁺ release.



INTRODUCTION

Organosilica nanoparticles represent a new class of nanoparticles obtained from polytriethoxysilyl-functionalized organic precursors without the presence of silica precursors. Organosilica nanoparticles are very different in terms of properties (hydrophilicity–lipophilicity, surface charge, loading capacity...) from the well-known silica nanoparticles. Organosilica nanoparticles possess attractive features particularly for bioapplications as recently reviewed.^{1,2} Porous organosilica nanoparticles^{3–5} and hollow systems,⁶ which offer new possibilities for drug adsorption and delivery, have also been reported and recently reviewed as well. However, the synthesis of porous organosilica nanoparticles with functional precursors is still a challenge, and for hollow systems, sophisticated procedures such as hard-core templating methods, liquid-interface assembling strategies (using FC-4 surfactant), reassembly methods, or synthesis procedures involving a prehydrolysis step of the organosilanes have been proposed.^{6,7} Stimuli-triggered degradability has also been studied with organosilica nanoparticles, particularly by bridging the structure with disulfides,^{7,8} which leads to the breaking of the nanoparticles by redox reaction with glutathione (GSH). The degradability of nanoparticles is indeed important for their safe elimination from the body.^{8–10} In addition, redox-responsive vectors can react with the high intracellular level of GSH and significantly improve drug concentrations in targeted cells, improving the therapeutic efficiency with a decrease of the side-effects of primary drugs.^{11,12} Concerning

applications, the main field is anticancer research, but a recent example was described with organosilica nanoparticles able to release reactive oxygen species and NO upon sunlight irradiation for antibacterial activity.¹³ In this context, we were interested in new hollow organosilica nanoparticles, which are able to be degraded upon treatment with GSH for antibacterial applications to improve their in vivo elimination. In this case, the precursors bis(trimethoxysilylpropyl)methylamine (BMSPMA) and bis(trimethoxysilylpropyl)disulfide (DIS) were condensed with the O/W microemulsion method, with cetyltrimethylammonium bromide (CTAB) as the template, using the sol–gel method in basic media. The obtained hollow degradable organosilica nanoparticles (HDOSNPs) were then loaded with silver ions and amoxicillin, with a high loading capacity. Treatment of *Escherichia coli* colonies led to an efficient inhibition of the growth of the bacteria because of the synergic effect of the drug (amoxicillin) and the adjuvant (silver ions).

MATERIALS AND METHODS

CTAB (99%), sodium hydroxide (97%), BMSPMA, and DIS were purchased from Sigma-Aldrich. UV–vis absorption spectra were recorded on a Hewlett-Packard 8453 spectrophotometer. ²⁹Si solid-state NMR spectra were recorded on a

Received: October 12, 2018

Accepted: December 18, 2018

Published: January 17, 2019

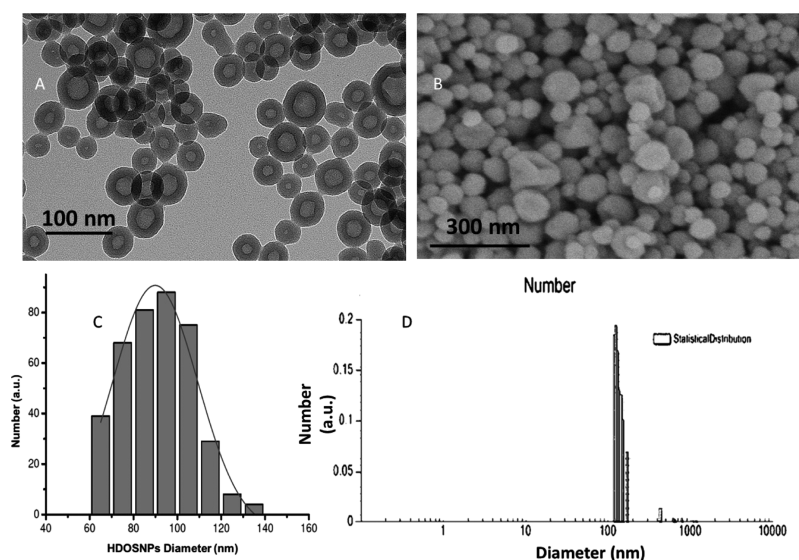


Figure 1. Characterizations of the HDOSNP sample. (A) TEM and (B) SEM images. (C) Size distribution from TEM measurements. (D) DLS of HDOSNPs in EtOH.

Varian VNMRS 300 MHz NMR spectrometer, using a 3.2 mm magic angle spinning (MAS) probe spinning at 6 kHz. The operating frequencies for ^1H and ^{29}Si were 300.00 and 59.59 MHz, respectively. A ^1H – ^{29}Si cross-polarization MAS (CP-MAS) NMR experiment was performed, using a contact time of 5 ms. “ Q_8MH_8 ” was used as a secondary reference (low-frequency peak at -109.2 ppm). ^{13}C solid-state NMR experiments were performed on a Varian VNMRS 600 MHz (14.1 T) NMR spectrometer, using a 3.2 mm Varian T3 HXY MAS probe tuned to ^1H (599.81 MHz) and ^{13}C (150.84 MHz). One-dimensional ^1H – ^{13}C CP-MAS NMR spectra were recorded by spinning at 18 kHz, using a 90° ^1H excitation pulse of 2.5 μs , followed by a contact time of 3 ms (ramped pulse). ^{13}C chemical shifts were referenced externally to adamantane (used as a secondary reference), the high-frequency peak being set to 38.5 ppm. N_2 adsorption isotherms were measured at 77 K using a TriStar 3000 gas adsorption analyzer instrument, and the specific surface area was determined using the Brunauer–Emmett–Teller (BET) method. X-ray powder diffraction analyses were performed on a PANalytical X’Pert Pro MPD diffractometer with $K\alpha$ radiation of Cu ($\lambda = 1.5418$ Å). Zeta potentials were measured using Malvern Zetasizer Nano Series. Transmission electron microscopy (TEM) was carried out with a Tecnai 12 T (FEI Co.) microscope operated at 120 kV. Dynamic light scattering (DLS) analyses were performed using a Cordouan Technologies DL 135 particle size analyzer instrument. Inductively coupled plasma–atomic emission spectroscopy (ICP–AES) was performed with a PerkinElmer 7000 DV Optima Instruments. TEM analysis was performed on a JEOL 1200 EXII instrument. Scanning electron microscopy (SEM) was used to investigate the nanoparticle morphology. A drop of the suspension containing the nanoparticles was deposited on a microscope grid, coated with a gold film, and examined using an FEI Inspect F50 high-resolution SEM instrument operated at an accelerating voltage of 20 kV.

Synthesis of HDOSNPs. A mixture of CTAB (6.4 mg, 1.6×10^{-5} mol), ultrapure water (20 mL), absolute ethanol (100 μL), and sodium hydroxide (13 μL , 1 M) was stirred at 75°C for 50 min at 1000 rpm in a three-neck glass flask. In the

meantime, 12.5 μL of BMSPPMA was diluted in 9 mL of ethanol and sonicated for 30 min and 18.10 μL of DIS was added according to the molar ratio of two precursors BMSPPMA/DIS (50:50) and left to sonicate for 10 more minutes. The reaction was started by the addition of solution of precursors, followed by the change of conditions to 80°C (1400 rpm). The reaction mixture was stirred for 2 h, cooled to room temperature, and centrifuged at 15 min at 20 000 rpm. Micelles of CTAB were removed by three time extraction with a 0.075 M solution of ammonium nitrate in ethanol, followed by three ethanol washes. Biodegradable organosilica nanoparticles were then dried under vacuum at room temperature.

Amoxicillin Loading of the HDOSNPs in Acidic Conditions (pH \approx 5.5). A mixture of HDOSNPs (10 mg), amoxicillin (3 mg), and deionized water (1 mL) was prepared in an Eppendorf tube and 3 μL of hydrochloric acid (10^{-3} M) was added to reach pH \approx 5.5. Then, the suspension was stirred overnight at room temperature. The solution was neutralized with 3 μL of sodium hydroxide (10^{-3} M) and stirred for 30 min. Finally, the NPs were collected by centrifugation (10 000 rpm, 5 min). The sample was washed two times with water and dried 1 day under air. The loading and washing solution supernatants were retained to determine the amoxicillin payloads. The amoxicillin loading determined with the loading solution supernatants was 17 wt % (the sample is labeled Amox₁₇@HDOSNPs).

Silver Ion Loading of the HDOSNPs in Water. A mixture of NPs (10 mg), silver nitrate (AgNO_3 , 5 mg), and deionized water (1 mL) was prepared in an Eppendorf tube. Then, the suspension was stirred overnight at room temperature. The NPs were collected by centrifugation (10 000 rpm, 15 min). The sample was washed three times with water and dried 1 day under air. A gray solid was obtained (the sample is denoted HDOSNPs– Ag_x^+ , where x represents the silver loading in wt %).

Amoxicillin and Silver Ion Loading of the HDOSNPs in Acidic Conditions (pH \approx 5.5). A mixture of HDOSNPs (10 mg), amoxicillin (5 mg), silver nitrate (AgNO_3 , 5 mg), and deionized water (1 mL) was prepared in an Eppendorf tube and 3 μL of hydrochloric acid (10^{-3} M) was added to reach

pH \approx 5.5. Then, the suspension was stirred overnight at room temperature. The solution was neutralized with 3 μ L of sodium hydroxide (10^{-3} M) and stirred for 30 min. Finally, the NPs were collected by centrifugation (14 000 rpm, 15 min). The sample was washed two times with water and dried 1 day under air. The loading and washing solution supernatants were retained to determine the amoxicillin payloads. The amoxicillin loading determined with the loading solution supernatants was 30 wt %. A black solid was obtained (the sample is denoted Amox₃₀@HDOSNPs-Ag_x⁺).

ICP–AES Titration. Four milligrams of Amox₃₀@HDOSNPs-Ag_x⁺ or HDOSNPs-Ag_x⁺ was dispersed in 3 mL of concentrated HNO₃ (86%, 1 mL), H₂SO₄ (95%, 1 mL), and HF (60%, 1 mL). The mixture was heated at 50 °C until dissolution. The residue was dissolved in 25 mL of water and the solution was analyzed.

Bactericidal Activity. Gradient concentrations of NPs (10, 20, and 50 μ g/mL) were added to the culture medium in the presence of 10⁸ colony forming units (CFU)/mL of *E. coli* bacteria (DH5 α). Bacteria/NP mixed cultures were tested using a microplate reader at 37 °C. At intervals of 1 h, optical density (OD) at 600 nm was determined for bacterial cell growth.

RESULTS AND DISCUSSION

The monodisperse HDOSNPs were prepared through the condensation of BMSPMA and DIS in water/ethanol solution using CTAB as the structure-directing agent in basic media. The sol–gel process was carried out for 2 h at 75 °C in highly diluted conditions with sodium hydroxide as the catalyst. Then, the surfactant was extracted three times with an ethanolic mixture of ammonium nitrate, and the remaining HDOSNPs were washed three times with ethanol. Each extraction step involved a sonication of 30 min at 40 °C. The as-prepared material was dried under vacuum for few hours.

The HDOSNPs were then characterized by TEM and SEM (Figure 1A,B), showing 100 nm monodisperse hollow spherical nanoparticles with wall size of about 10 nm. The size distribution obtained by TEM was centered at 90 nm as shown in Figure 1C.

The size distribution and monodispersity of the nanoparticles was confirmed by DLS measurements and was centered at 150 nm in EtOH with few aggregates due to the drying process (Figure 1D).

Solid-state ²⁹Si CP-MAS NMR showed the presence of signals at –58 and –68 ppm, corresponding to ²T and ³T units of the well-condensed siloxane network, respectively, (Figure 2A). NMR ¹³C CP-MAS spectra (Figure 2B) clearly confirmed the presence of the carbons found in BMSPMA at 10, 21, 43, and at 64 ppm with the carbons found in DIS at 10, 28, and 48 ppm.

Low- and wide-angle X-ray diffraction (XRD) patterns (Figure 3) showed a disorder structure at low angle, as there is no periodicity in the porosity and the characteristic siloxane network at wide angle at $2\theta = 20^\circ$, respectively.

The zeta potential of HDOSNPs was studied in simulated physiologic conditions at pH 7.4 (as in the blood stream) by dilution in NaCl (1 mM). The value was 25 mV, in agreement with the protonation of the amine groups.

Microanalysis was performed and showed the presence of nitrogen (5.1%) and sulfur (1.2%), in agreement with the condensation of both DIS and BMSPMA. The higher content

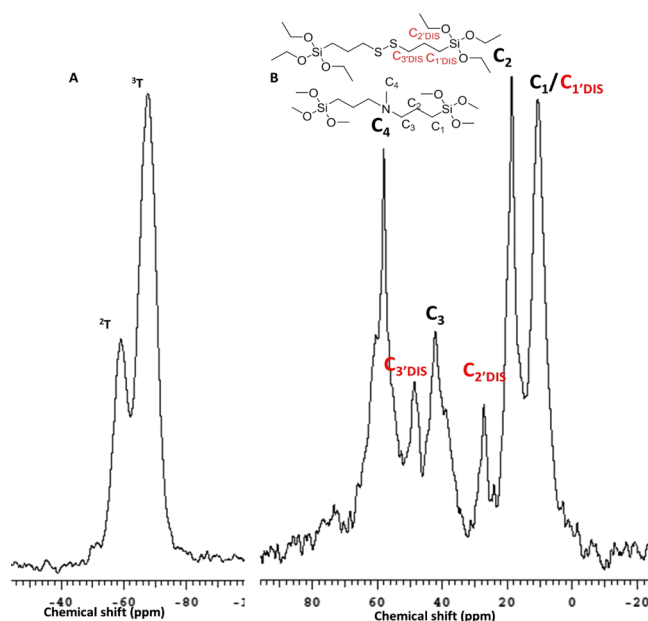


Figure 2. (A) ²⁹Si CP-MAS solid-state NMR and (B) ¹³C CP-MAS solid-state NMR of HDOSNPs.

with N compared to S is consistent with the residual adsorption of ammonium nitrate used to extract the surfactant.

HDOSNPs were then subjected to adsorption measurements to get information about their textural and surface chemistry properties. Nitrogen sorption was performed after synthesis, on the pristine material and also after water and *n*-hexane vapor adsorption. The nitrogen adsorption isotherm is presented in Figure 4A. This adsorption isotherm principally belongs to the type II defined by the IUPAC, expressing multilayer adsorption, which corresponds to nonporous materials. The hysteresis loop present at high relative pressure is likely due to some interparticular adsorption in voids. These voids being generated by the agglomeration of nanoparticles of 50 nm diameter in average, their size is usually in the same order of magnitude. This is consistent with the location of the hysteresis loop ($p/p^0 > 0.9$) according to the Kelvin law. The external surface area of the pristine material can be calculated using a usual relationship. Our material being made of spherical particles, the external surface is $6/\rho d$.¹⁴ If the density ρ is taken as 2 g cm⁻³ and the mean particle diameter d is taken as 0.05 μ m, the external surface area is 60 m² g⁻¹. Despite the approximations made both on the density and particle morphology, this result is very close to the specific surface area derived using the BET model, that is, 56 m² g⁻¹. This consistency confirms that our material is mostly nonporous to nitrogen at 77 K, in agreement with the previously reported results concerning the restricted accessibility at cryogenic temperatures (77 K) of nitrogen molecules to internal volume and the surface of Stöber-like nanosilica.¹⁵ This leads to a deficient characterization of the nanoparticles due to adsorption of nitrogen only at the outer particle surface. The C_{BET} value, which is an indication of the affinity between HDOSNPs and nitrogen, was found to be 127. This value is higher than that usually found for nonporous pure silicas ($C_{\text{BET}} < 40$),¹⁶ which is indicative of an interaction between nitrogen and organic moieties of the hybrid material. The strong adsorption of the nitrogen probe with the surface sites of the pore entrance was reported to prevent diffusion and adsorption

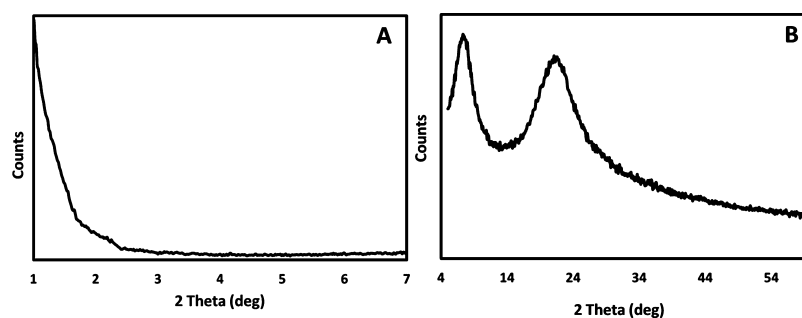


Figure 3. (A) Low-angle and (B) wide-angle XRD patterns of HDOSNPs.

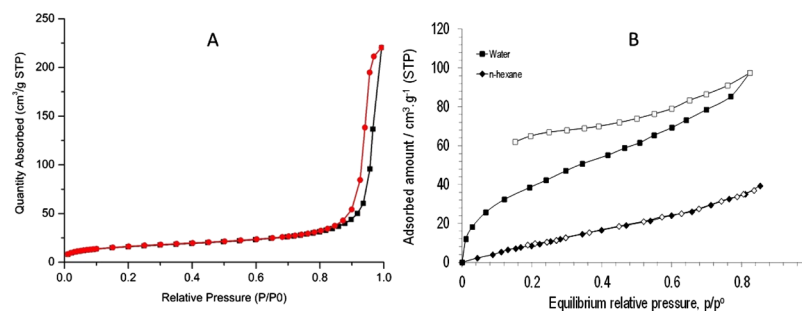


Figure 4. (A) N_2 adsorption–desorption isotherms of HDSNP. (B) *n*-Hexane and water vapor adsorption determined at 313 K. Adsorption: filled symbols; desorption: empty symbols.

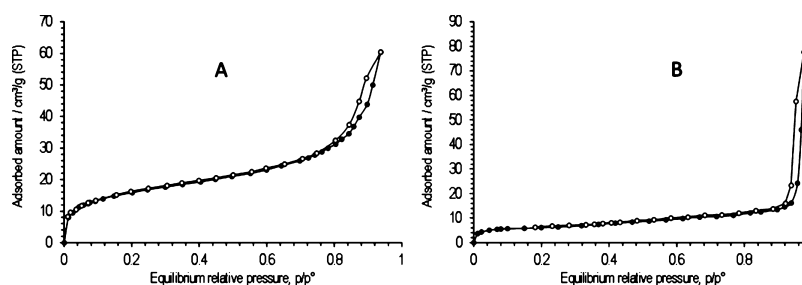


Figure 5. Nitrogen adsorption determined at 77 K (A) after *n*-hexane adsorption and (B) after water adsorption. Adsorption: filled symbols; desorption: empty symbols.

inside the pore (mechanism of activated entry).¹⁷ A relevant assessment of the specific surface area and pore characterization are however possible from water adsorption performed on the pristine material. Indeed, the studies of water adsorption isotherms proved that a large amount of water can fill the microporous volume of Stöber-like nanosilica.¹⁸ Considering the small kinetic diameter of H_2O (0.265 nm) compared to 0.360 nm for N_2 , it was reported that water adsorption in silicas can detect the microporosity while N_2 adsorption could not.¹⁸ Vapor adsorption was also performed for evaluating the hydrophilic/lipophilic balance of the material. Water and *n*-hexane adsorption isotherms are presented in Figure 4B.

In the case of *n*-hexane sorption, a rather linear and reversible adsorption desorption is observed. The linear character of the trace can be interpreted as a sorption process occurring on a homogeneous surface in terms of interaction. This Henry's type of behavior can be understood by considering that *n*-alkanes only generate van der Waals interaction, whose extent depends on the size of the *n*-alkane.¹⁹ The reversibility of the sorption process confirms that *n*-hexane only generates physisorption. Additionally, it can be deduced that after sorption, the material remains unchanged.

In the case of water, the sorption isotherm obtained is very different. The adsorption branch exhibits a clear curvature at low relative pressure, indicative of a good affinity between water and HDOSNPs. Furthermore, the adsorbed amounts are larger than those in the case of *n*-hexane, which means that water interacts with more surface sites than *n*-hexane. Moreover, the large hysteresis loop indicates that the sorption process is not reversible, suggesting that the water/surface interactions with amine groups (hydrogen bonds) are rather strong. The specific surface area accessed by the water molecules reached $107 \text{ m}^2 \text{ g}^{-1}$, determined from the water adsorption isotherm (Figure 4B) at 313 K using the BET equation and considering a cross-sectional area of 0.105 nm^2 for the water molecule. Moreover, the micropore volume for H_2O was calculated using the Dubinin–Radushkevich equation applied to the water isotherm (Figure 4B). Thus, a microporous volume V_{H_2O} of 0.043 cm^3 was obtained, expressed considering H_2O as a liquid with a density of 0.997 g cm^{-3} (value used for the calculations), which corresponds to approximately 10% of the organosilica nanosphere volume ($\rho \approx 2 \text{ g cm}^{-3}$). In summary, the accessibility of water to the inner micropores of HDOSNPs

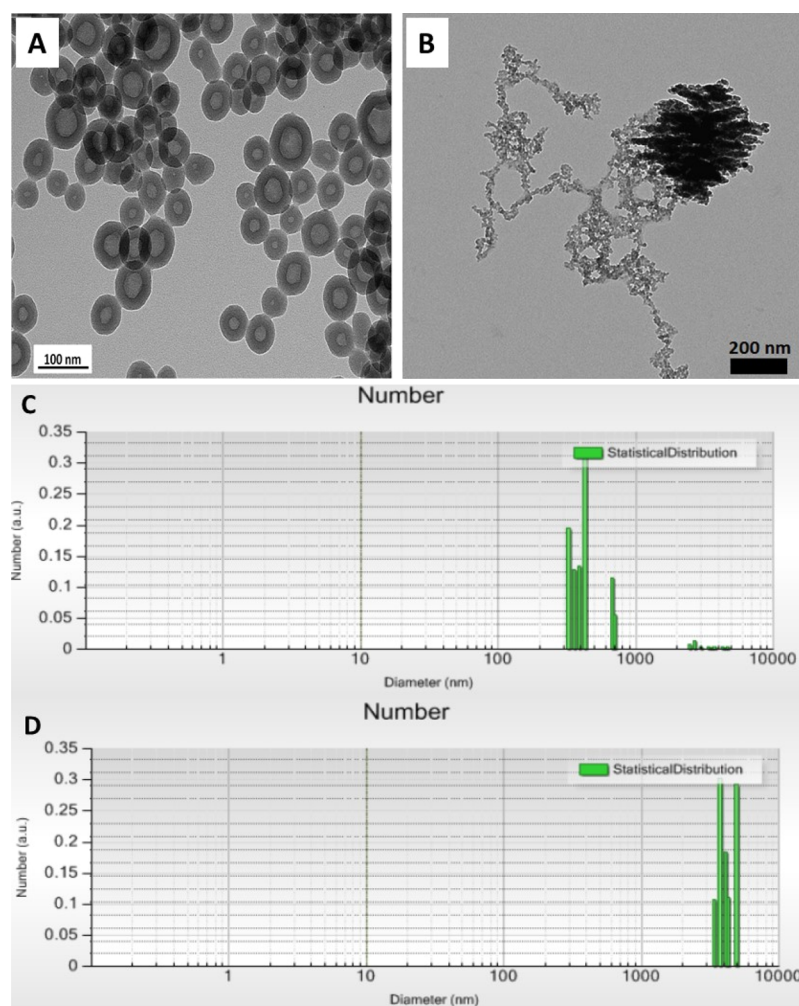


Figure 6. TEM images before (A) and after (B) 48 h treatment of HDOSNPs with EtSH. DLS before (C) and after (D) 48 h treatment of HDOSNPs with EtSH in PBS at 37 °C.

was highlighted. The microporosity arose from the presence of CTAB surfactant micelles in the reaction medium constituted here of a water/ethanol mixture. Indeed, the porosity of the surfactant-templated materials is linked directly to the micelle size used as the porogen. However, a decrease of both the surfactant aggregation number and the micellar size was highlighted by increasing the amount of polar alcohol (methanol, ethanol, ethylene glycol, glycerol...) into the aqueous reaction media.^{20–22} As a result, the final porosity of HDOSNPs was thus shrunk compared with that reported for MSN-type particles.

The integrity of the material after vapor adsorption was also investigated by nitrogen adsorption, and the results are shown in Figure 5.

The nitrogen adsorption isotherm obtained after *n*-hexane sorption is very similar to that obtained with the pristine material. This confirms that *n*-hexane sorption is reversible and keeps the material unchanged. On the contrary, the nitrogen adsorption isotherm obtained after water adsorption shows very low adsorbed amounts, emphasizing the irreversible action of water toward HDOSNPs as discussed above. The inflexion at low relative pressure remains, which suggests that the used material still has some active surface sites, which are able to interact with nitrogen.

As the proof of concept of the biodegradability of disulfide-based bridged silsesquioxane nanoparticles was previously reported,²³ an enhanced degradability under the same conditions for the investigated hollow disulfide-based nanoparticles is also expected. The degradability of the HDOSNPs was assessed in near-physiological conditions in phosphate-buffered saline (PBS) at 37 °C. For this purpose, 1 mM of mercaptoethanol was added as an equivalent of the intracellular concentration of GSH. TEM images of the HDOSNPs before and after 48 h displayed the degradation of the HDOSNPs in the reducing solution (Figure 6A,B). DLS showed large aggregates of nanoparticles after degradation (Figure 6D) compared to the starting solution in PBS (Figure 6C).

HDOSNPs were loaded with amoxicillin in aqueous solution at pH 5.5 and RT. The loading capacity of Amox₁₇@HDOSNPs with amoxicillin was 17 wt %. The loading of HDOSNPs-Ag⁺ with Ag⁺ was performed in aqueous solution at RT and was 1.0 wt % as titrated by ICP–AES. Complementary, amoxicillin and Ag⁺ ions were both loaded with HDOSNPs at pH 5.5. An increase of the loading capacity of amoxicillin to 30 wt % was noticed with Amox₃₀@HDOSNPs-Ag⁺. The loading of Ag⁺ ions with Amox₃₀@HDOSNPs-Ag⁺ was 0.8 wt % as titrated by ICP–AES. The high Ag⁺ content suggests that silver Ag⁺ cations have reacted by complexation

with the disulfide moieties dispersed into the whole structure of HDOSNPs. Moreover, the immobilized silver ions represent from 70 to 80% of the sulfur amount in the HDOSNP structure based on the measured ratio of sulfur (1.2%). These results clearly show the accessibility of the internal structure toward silver ions. It is also expected that the amoxicillin molecules are adsorbed into the pore of the microporous structure of HDOSNPs. The integrity of Amox₃₀@HDOSNPs-Ag⁺ was checked by SEM as shown in Figure 7. This image

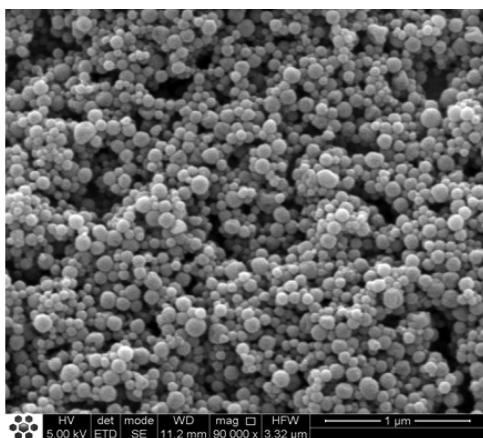


Figure 7. SEM image of Amox₃₀@HDOSNPs-Ag_{0.8}⁺.

clearly indicates that the overall nanoparticle structure was not affected by the loading process. Moreover, the spherical morphology of the nanoparticles was maintained even after the addition of silver ions in the composition of the material, which did not induce the disulfide bond cleavage. In the present study, silver ions (Ag⁺) are good antibiotic adjuvant candidates because of their wide antibacterial activity.²⁴ It was reported that release of Ag⁺ from the crystalline core of silver nanoparticles was the molecular toxicant,²⁵ which induces morphological and structural changes on *E. coli* and *Staphylococcus aureus* bacteria strains.²⁶ Moreover after Ag⁺ treat-

ment, DNA lost its replication ability and the protein became inactivated.²⁷

Nanoparticle Effect on Bacterial Growth. Functionalized organosilica nanoparticles had their antimicrobial ability tested against *E. coli*, which is commonly used as a model of Gram-negative bacteria. Experiments were performed by incubating distinct nanoparticles (at different concentrations) together with bacteria suspensions. Then, the OD, measured at 600 nm, was followed giving an indication of the bacterial growth. All experiments were performed for 20 h and the OD increase indicates the bacteria growth. The time-dependent changes in the microbial growth for distinct concentrations are presented in Figure 8A for the Amox₃₀@HDOSNPs-Ag₁⁺ sample. The HDOSNPs-Ag_{0.8}⁺ sample presented a similar behavior to the one shown here, whereas a much less pronounced inhibitory effect was observed for the Amox₁₇@HDOSNPs sample.

The comparison between distinct synthesized materials, considering 50 ppm sample concentration, is shown in Figure 8B where changes among the samples can be seen. To quantitatively evaluate these differences, the OD at 20 h of bacterial growth (last measured point in Figure 8C) was considered. The OD at this point can be clearly correlated with the ability on inhibiting *E. coli* proliferation, which was then normalized toward the bacterial growth of the control done in the absence of nanoparticles and antibiotic. There is no statistical difference between the positive control, HDOSNPs, and Amox₁₇@HDOSNPs. Although curious, the very low amount of antibiotic entrapped in Amox₁₇@HDOSNPs was not enough to make changes in the bacterial growth. Similar behaviors were already reported for various drug-loaded nanoparticles.^{28–30} A subtle and minor amount of silver ions of HDOSNPs-Ag_{0.8}⁺ was able to significantly and statistically reduce *E. coli* growth when compared to the HDOSNPs and Amox₁₇@HDOSNPs. Conversely, the bifunctionalized nanoparticles (Amox₃₀@HDOSNPs-Ag₁⁺) had a stronger inhibitory effect than the corresponding silver ion-loaded or amoxicillin-loaded samples. We suggest that this significant inhibitory

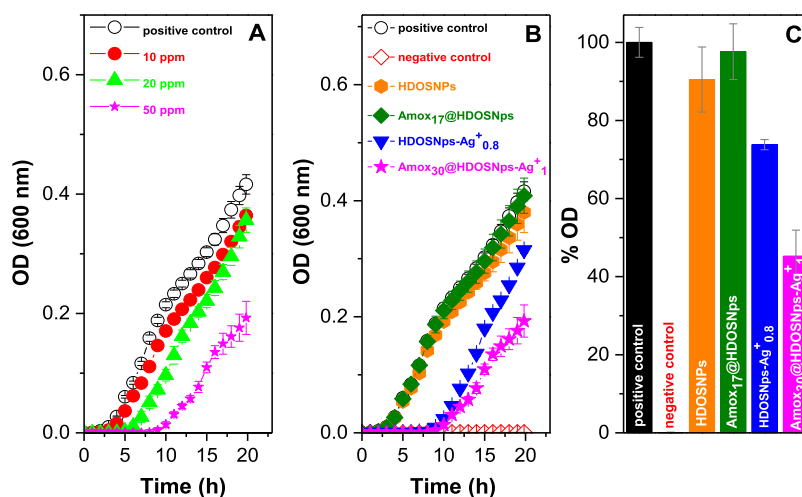


Figure 8. (A) Growth profiles of *E. coli* in MHB medium alone as positive controls (black circles and line) and in the presence of Amox₃₀@HDOSNPs-Ag₁⁺ nanoparticles at three concentrations (10, 20, 50 ppm). (B) Growth profiles of *E. coli* in MHB medium (positive control), in the presence of tetracycline (6 ppm, negative control), HDOSNPs (50 ppm), HDOSNPs-Ag_{0.8}⁺ (50 ppm), Amox₃₀@HDOSNPs-Ag₁⁺ (50 ppm), and Amox₁₇@HDOSNPs (50 ppm). (C) Bar graphs illustrate the percentage of surviving *E. coli* bacteria, obtained by OD measurement (at 600 nm) after 20 h of incubation with 50 ppm of the synthesized nanoparticles. The OD measure was compared with the positive control. Error bars represent the standard deviation.

effect, at a low concentration of 50 ppm, might be explained by a codelivery of silver ions and amoxicillin using multifunctional Amox₃₀@HDOSNPs-Ag₁⁺ nanoparticles adsorbed on the peptidoglycan region of the bacteria outer membrane. This codelivery hypothesis is well sustained by other materials already reported in the literature^{31–33} and highlights the enormous biological potential of the nanoparticles synthesized here. It is obvious that other adjuvants and antibiotics might be used to even increase the bactericidal activity or tune nanoparticles' properties for future biomedical applications.

CONCLUSIONS

In conclusion, we have successfully synthesized hollow disulfide bridge-based organosilica nanoparticles of about 100 nm diameter by using DIS and BMPMA precursors. These nanoparticles were nonporous at 77 K as shown by nitrogen adsorption-desorption analysis. *n*-Hexane showed a reversible adsorption-desorption with these nanoparticles, whereas a strong interaction was noticed with water when water was adsorbed. Amoxicillin was loaded with HDOSNPs with a loading capacity of 30%. Furthermore, silver ions and amoxicillin were also adsorbed with HDOSNPs and the loaded nanoparticles were very efficient in inhibiting bacterial growth due to a synergy between the antibiotic delivery and the adjuvant release.

AUTHOR INFORMATION

Corresponding Author

*E-mail: clarence.charnay@umontpellier.fr.

ORCID

Mateus Borba Cardoso: 0000-0003-2102-1225

Philippe Trens: 0000-0001-9162-8263

Jean-Olivier Durand: 0000-0003-4606-2576

Clarence Charnay: 0000-0002-8796-3701

Notes

The authors declare no competing financial interest.

ACKNOWLEDGMENTS

The Erasmus Mundus grant for S.R. is gratefully acknowledged. M.B.C. thanks the support of Fapesp (grant 2015/25406-5) and the productivity research fellowship granted by CNPq (grant no. 309107/2014-8) while K.B. acknowledges the support of Capes (CSF-PAJT-88887.091023/2014-00).

REFERENCES

- (1) Croissant, J. G.; Cattoën, X.; Durand, J.-O.; Wong Chi Man, M.; Khashab, N. M. Organosilica hybrid nanomaterials with a high organic content: syntheses and applications of silsesquioxanes. *Nanoscale* **2016**, *8*, 19945–19972.
- (2) Nakamura, M. Biomedical applications of organosilica nanoparticles toward theranostics. *Nanotechnol. Rev.* **2012**, *1*, 469–491.
- (3) Du, X.; Li, X.; Xiong, L.; Zhang, X.; Kleitz, F.; Qiao, S. Z. Mesoporous silica nanoparticles with organo-bridged silsesquioxane framework as innovative platforms for bioimaging and therapeutic agent delivery. *Biomaterials* **2016**, *91*, 90–127.
- (4) Chen, Y.; Shi, J. Chemistry of Mesoporous Organosilica in Nanotechnology: Molecularly Organic-Inorganic Hybridization into Frameworks. *Adv. Mater.* **2016**, *28*, 3235–3272.
- (5) Croissant, J. G.; Cattoën, X.; Wong Chi Man, M.; Durand, J.-O.; Khashab, N. M. Syntheses and applications of periodic mesoporous organosilica nanoparticles. *Nanoscale* **2015**, *7*, 20318–20334.

(6) Teng, Z.; Li, W.; Tang, Y.; Elzatahry, A.; Lu, G.; Zhao, D. Mesoporous Organosilica Hollow Nanoparticles: Synthesis and Applications. *Adv. Mater.* **2018**, 1707612.

(7) Sun, Y.; Chen, M.; Wu, L. Controllable synthesis of hollow periodic mesoporous organosilica spheres with radial mesochannels and their degradable behavior. *J. Mater. Chem. A* **2018**, *6*, 12323–12333.

(8) Du, X.; Kleitz, F.; Li, X.; Huang, H.; Zhang, X.; Qiao, S.-Z. Disulfide-Bridged Organosilica Frameworks: Designed, Synthesis, Redox-Triggered Biodegradation, and Nanobiomedical Applications. *Adv. Funct. Mater.* **2018**, *28*, 1707325.

(9) Croissant, J. G.; Fatieiev, Y.; Khashab, N. M. Degradability and Clearance of Silicon, Organosilica, Silsesquioxane, Silica Mixed Oxide, and Mesoporous Silica Nanoparticles. *Adv. Mater.* **2017**, *29*, 1604634.

(10) Croissant, J. G.; Fatieiev, Y.; Almalik, A.; Khashab, N. M. Mesoporous Silica and Organosilica Nanoparticles: Physical Chemistry, Biosafety, Delivery Strategies, and Biomedical Applications. *Adv. Healthcare Mater.* **2018**, *7*, 1700831.

(11) Chen, Y.; Meng, Q.; Wu, M.; Wang, S.; Xu, P.; Chen, H.; Li, Y.; Zhang, L.; Wang, L.; Shi, J. Hollow Mesoporous Organosilica Nanoparticles: A Generic Intelligent Framework-Hybridization Approach for Biomedicine. *J. Am. Chem. Soc.* **2014**, *136*, 16326–16334.

(12) Guo, X.; Cheng, Y.; Zhao, X.; Luo, Y.; Chen, J.; Yuan, W.-E. Advances in redox-responsive drug delivery systems of tumor microenvironment. *J. Nanobiotechnol.* **2018**, *16*, 74.

(13) Gehring, J.; Trepka, B.; Klinkenberg, N.; Bronner, H.; Schleheck, D.; Polarz, S. Sunlight-triggered nanoparticle synergy: Teamwork of reactive oxygen species and nitric oxide released from mesoporous organosilica with advanced antibacterial activity. *J. Am. Chem. Soc.* **2016**, *138*, 3076–3084.

(14) Rouquerol, F.; Rouquerol, J.; Sing, K. *Adsorption by Powders and Porous Solids: Principles, Methodology and Applications*; Academic, 1999; p 467.

(15) Szekeres, M.; Tóth, J.; Dékány, I. Specific Surface Area of Stoeber Silica Determined by Various Experimental Methods. *Langmuir* **2002**, *18*, 2678–2685.

(16) Gregg, S. J.; Sing, K. S. W. *Adsorption, Surface Area and Porosity*, 2nd ed.; Academic Press, 1982; p 303.

(17) Isobe, H.; Kaneko, K. Porous Silica Particles Prepared from Silicon Tetrachloride Using Ultrasonic Spray Method. *J. Colloid Interface Sci.* **1999**, *212*, 234–241.

(18) Farrando-Pérez, J.; López, C.; Silvestre-Albero, J.; Gallego-Gómez, F. Direct Measurement of Microporosity and Molecular Accessibility in Stöber Spheres by Adsorption Isotherms. *J. Phys. Chem. C* **2018**, *122*, 22008–22017.

(19) Trens, P.; Tanchoux, N.; Maldonado, D.; Galarneau, A.; Di Renzo, F.; Fajula, F. Study of *n*-hexane adsorption in MCM-41 mesoporous materials: a scaling effect approach of capillary condensation processes. *New J. Chem.* **2004**, *28*, 874–879.

(20) Li, W.; Zhang, M.; Zhang, J.; Han, Y. Self-assembly of cetyl trimethylammonium bromide in ethanol-water mixtures. *Front. Chem. China* **2006**, *1*, 438–442.

(21) Hamel, A.; Sacco, M.; Mnasri, N.; Lamaty, F.; Martinez, J.; De Angelis, F.; Colacino, E.; Charnay, C. Micelles into Glycerol Solvent: Overcoming Side Reactions of Glycerol. *ACS Sustainable Chem. Eng.* **2014**, *2*, 1353–1358.

(22) Nyalosaso, J. L.; Derrien, G.; Charnay, C.; de Menorval, L.-C.; Zajac, J. Aluminium-derivatized silica monodisperse nanospheres by a one-step synthesis-functionalization method and application as acid catalysts in liquid phase. *J. Mater. Chem.* **2012**, *22*, 1459–1468.

(23) Croissant, J. G.; Mauriello-Jimenez, C.; Maynadier, M.; Cattoën, X.; Wong Chi Man, M.; Raehm, L.; Mongin, O.; Blanchard-Desce, M.; Garcia, M.; Gary-Bobo, M.; Maillard, P.; Durand, J.-O. Synthesis of disulfide-based biodegradable bridged silsesquioxane nanoparticles for two-photon imaging and therapy of cancer cells. *Chem. Commun.* **2015**, *51*, 12324–12327.

(24) Morones-Ramirez, J. R.; Winkler, J. A.; Spina, C. S.; Collins, J. J. Silver enhances antibiotic activity against gram-negative bacteria. *Sci. Transl. Med.* **2013**, *5*, 190ra81.

(25) Xiu, Z.-m.; Zhang, Q.-b.; Puppala, H. L.; Colvin, V. L.; Alvarez, P. J. J. Negligible particle-specific antibacterial activity of silver nanoparticles. *Nano Lett.* **2012**, *12*, 4271–4275.

(26) Feng, Q. L.; Wu, J.; Chen, G. Q.; Cui, F. Z.; Kim, T. N.; Kim, J. O. A mechanistic study of the antibacterial effect of silver ions on *Escherichia coli* and *Staphylococcus aureus*. *J. Biomed. Mater. Res.* **2000**, *52*, 662–668.

(27) Feng, Q. L.; Wu, J.; Chen, G. Q.; Cui, F. Z.; Kim, T. N.; Kim, J. O. A mechanistic study of the antibacterial effect of silver ions on *Escherichia coli* and *Staphylococcus aureus*. *J. Biomed. Mater. Res.* **2000**, *52*, 662–668.

(28) Alvarez, G. S.; H elary, C.; Mebert, A. M.; Wang, X.; Coradin, T.; Desimone, M. F. Antibiotic-loaded silica nanoparticle-collagen composite hydrogels with prolonged antimicrobial activity for wound infection prevention. *J. Mater. Chem. B* **2014**, *2*, 4660–4670.

(29) Zheng, F.; Wang, S.; Wen, S.; Shen, M.; Zhu, M.; Shi, X. Characterization and antibacterial activity of amoxicillin-loaded electrospun nano-hydroxyapatite/poly(lactic-co-glycolic acid) composite nanofibers. *Biomaterials* **2013**, *34*, 1402–1412.

(30) Azhdarzadeh, M.; Lotfipour, F.; Zakeri-Milani, P.; Mohammadi, G.; Valizadeh, H. Anti-bacterial performance of azithromycin nanoparticles as colloidal drug delivery system against different gram-negative and gram-positive bacteria. *Adv. Pharm. Bull.* **2012**, *2*, 17–24.

(31) Bouchmella, K.; Campanaro, F. D.; Mondo, G. B.; Santos, M. I.; Franco, C. H.; Moraes, C. B.; Biolley, C.; Mehdi, A.; Cardoso, M. B. Tetracycline@silver ions-functionalized mesoporous silica for high bactericidal activity at ultra-low concentration. *Nanomedicine* **2018**.13 DOI: 10.2217/nnm-2018-0027

(32) Lu, M.; Wang, Q.; Chang, Z.; Wang, Z.; Zheng, X.; Shao, D.; Dong, W.; Zhou, Y. Synergistic bactericidal activity of chlorhexidine-loaded, silver-decorated mesoporous silica nanoparticles. *Int. J. Nanomed.* **2017**, *12*, 3577–3589.

(33) de Oliveira, J. F. A.; Saito,  . A.; Bido, A. T.; Kobarg, J.; Stassen, H. K.; Cardoso, M. B. Defeating Bacterial Resistance and Preventing Mammalian Cells Toxicity Through Rational Design of Antibiotic-Functionalized Nanoparticles. *Sci. Rep.* **2017**, *7*, 1326.